

Precise Time Delay Measurement and Compensation for Tightly Coupled Underwater SINS/piUSBL Navigation

Jin Huang¹, Graduate Student Member, IEEE, Yingqiang Wang², Member, IEEE, Haoda Li², Zichen Liu²,
Zhikun Wang³, Ying Chen³

Abstract—In multi-sensor systems, time synchronization between sensors is a significant challenge, and this issue is particularly pronounced in underwater integrated navigation systems incorporating acoustic positioning. Such systems are highly susceptible to time delay, which can significantly degrade accuracy when measurement and fusion moments are misaligned. To address this challenge, this paper introduces a tightly coupled navigation framework that integrates a passive inverted ultra-short baseline (piUSBL) acoustic positioning system, a strapdown inertial navigation system (SINS), and a depth gauge under precise time synchronization. The framework fuses azimuth and slant range from the piUSBL with depth data, thereby avoiding poor vertical-angle observability in planar arrays. A novel delay measurement strategy is introduced, combining synchronized timing with acoustic signal processing, which redefines delay—traditionally an unobservable error—into a quantifiable parameter, enabling explicit estimation of both acoustic propagation and system processing delays. Simulations and field experiments confirm the feasibility of the proposed method, with delay-compensated navigation reducing RMSE by 40.45% and maximum error by 32.55%. These findings show that precise delay measurement and compensation not only enhance underwater navigation accuracy but also establish a generalizable framework for acoustic positioning integration, offering valuable insights into time alignment and data fusion in latency-sensitive multi-sensor systems.

Index Terms—Underwater navigation, passive inverted ultra-short baseline (piUSBL), integrated navigation system (INS), clock synchronization, time delay measurement.

I. INTRODUCTION

AUTONOMOUS Underwater Vehicles (AUVs) are widely employed in various underwater applications, such as marine environment monitoring, underwater archaeology, and offshore structure inspection [1], [2]. Due to the significant attenuation of electromagnetic signals in underwater environments, Global Navigation Satellite System (GNSS) signals cannot provide accurate positioning information for AUVs [3]. In GNSS-denied environments, the strapdown inertial navigation system (SINS) is commonly used to provide continuous navigation information for AUVs [4]. However, the SINS is prone to error accumulation, leading to drift in the navigation solution over time [5]. To address this issue, various aiding systems have been developed to assist the SINS and reduce

drift errors, such as the Doppler velocity log (DVL), acoustic positioning systems, and altimeters [6], [7].

Among various aiding systems, acoustic positioning system is widely used in underwater navigation due to its high accuracy and reliability. The most common acoustic positioning systems are the long baseline (LBL), short baseline (SBL), and ultra-short baseline (USBL) systems [8]. Of these, the USBL system is the most popular, primarily because of its compact size and ease of deployment on AUVs [9], [10]. To adapt to the expanding operational scenarios of AUVs, innovative USBL system derivations like inverted USBL (iUSBL) system and passive inverted USBL (piUSBL) system have been introduced [11], [12]. In contrast to the conventional USBL system, the iUSBL architecture mounts the transducer array directly on the submersible, eliminating the need for position acquisition via acoustic communication with the surface vessel, which traditionally determines the relative position through two-way travel time (TWTT) measurements [13], [14]. Building upon the iUSBL system, the piUSBL further introduces time synchronization and adopts a one-way travel time (OWTT) scheme for positioning [15].

Due to the relatively slow speed of sound propagation underwater, typically around 1500 m/s, the position information obtained from acoustic positioning systems often experiences delays ranging from several hundred milliseconds to a few seconds [16]. For an integrated navigation system (INS) using inertial measurement unit (IMU) with sampling rates exceeding 200 Hz, these delays can accumulate significant errors and compromise system accuracy if not properly addressed [17], [18].

Research on this issue can be broadly categorized into two directions: estimating the delay and compensating for the delay. The first direction focuses on estimating or eliminating the observed time delay. The method typically augments the state vector with a delay variable, estimates the delay using slant range and vehicle velocity information, and then applies compensation directly [19], [20]. In addition, inspired by GNSS, a dual-beacon/hydrophone differential method eliminates the common errors by differencing the measurements from two beacons/hydrophones, which includes the clock measurement bias, transponder delay, and sound speed error [21], [22]. Despite their effectiveness, these methods do not analyze the observability of the time delay in the error state model, and the accuracy of time estimation remains uncertain. In differential approaches, the inter-system delay and observability issues also require further study.

The second direction assumes that the delay is already

Corresponding author: Yingqiang Wang and Ying Chen.

Jin Huang, Haoda Li, Zichen Liu, and Ying Chen are with the Ocean College, Zhejiang University, Zhoushan, 316021, China.

Yingqiang Wang is with the School of Oceanography, Shanghai Jiao Tong University, Shanghai, 200240, China.

Zhikun Wang is with the Donghai Laboratory, Zhoushan, 316021, China

known and focuses on designing filters that can properly process delayed sensor data. Existing strategies can be classified into two main categories. The first is retroactive processing, which revises past states using techniques such as filter recalculation (FR) [23], state inversion (SI) [24], or bounded circular buffers (BCB) to store historical states [25]. The second is real-time processing, where delayed observations are handled as they arrive. This includes approaches such as velocity aiding with DVL measurements, projecting delayed data onto the current state with adjusted measurement noise [26], or reconstructing historical states through state transition matrix inversion to form equivalent measurement updates [27]. Another representative method is the delay-state unscented Kalman filter (DS-UKF), which incorporates historical states into an extended state vector and processes them once the delayed measurements become available [28].

Overall, existing approaches predominantly rely on delay estimation and employ various techniques to filter measurements with inherent time delays. However, these methods typically focus on estimating sensor time delays for compensation, and the accuracy of these estimations, as well as the observability of delays within the error-state model, remains insufficiently explored. To address these challenges, this paper introduces a novel approach that integrates the piUSBL system. Unlike conventional acoustic positioning systems, the piUSBL system achieves inherently lower delay, providing a more efficient foundation for time synchronization [29]. More importantly, the proposed method goes beyond simply incorporating the piUSBL system, it combines precise time synchronization with the SINS through the synchronous clock in piUSBL system, enabling accurate timestamps for each stage of signal acquisition and processing and make it possible for measurement and compensation of delays throughout the navigation process. This integration addresses key limitations in prior approaches and offers a robust solution for time delay compensation. The main contributions of this paper are as follows:

1. A **SINS/piUSBL/depth gauge tightly integrated navigation system** is proposed. Rather than a simple sensor combination, the framework construct a minimal yet observable measurement model, using azimuth, slant range, and depth as complementary observations. This design not only overcomes the poor vertical-angle observability of planar arrays but also provides a methodological reference for extending low-complexity acoustic systems into rigorous navigation frameworks.
2. A **delay measurement approach** is developed to address time delays. By systematically integrating time synchronization with acoustic signal processing, the method offers a rigorous approach for accurately quantifying both acoustic propagation and system processing delays. This approach transforms delay, which is traditionally an unobservable error, into a quantifiable and compensable parameter, thereby enhancing the system's overall robustness and reliability.
3. **Comprehensive simulations and field experiments** are conducted to evaluate the theoretical and practical im-

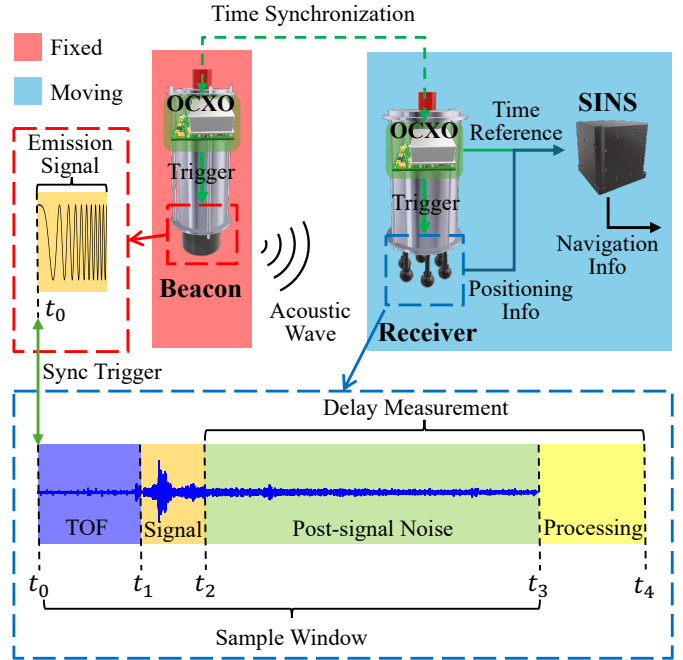


Fig. 1. The system architecture of the SINS/piUSBL tightly coupled navigation system with time synchronization.

plications of the proposed system. Simulations analyze the effect of time delays on the positioning accuracy of acoustic systems, demonstrating that the proposed delay compensation method significantly improves positioning performance, while field experiments confirm the method's validity. Together, these evaluations highlight not only empirical improvements but also the general applicability of the approach to delay-sensitive navigation scenarios.

The rest of this paper is organized as follows: Section II introduces the architecture of the proposed tightly coupled integrated navigation system with time synchronization. Section III presents the methodology, including the integrated navigation strategy utilizing precise time delay measurements and the SINS/piUSBL/depth gauge tightly coupled integrated navigation algorithm. Section IV describes the simulation and field experiments conducted to validate the proposed approach. Finally, Section V concludes the paper.

II. SYSTEM ARCHITECTURE

In most acoustic-aided integrated navigation systems, the acoustic subsystem operates independently and is loosely coupled with the overall system, which limits researchers' access to its raw data, such as per-channel signals and detailed processing procedures. In this paper, we propose a navigation framework that deeply integrates acoustic positioning with inertial navigation, realized through a tightly coupled SINS/piUSBL/depth gauge system with time synchronization. For simplicity, the term "SINS/piUSBL" is hereafter used to denote the SINS/piUSBL/depth gauge system.

Fig. 1 illustrates the essential components of the SINS/piUSBL integrated navigation system. The beacon is mounted

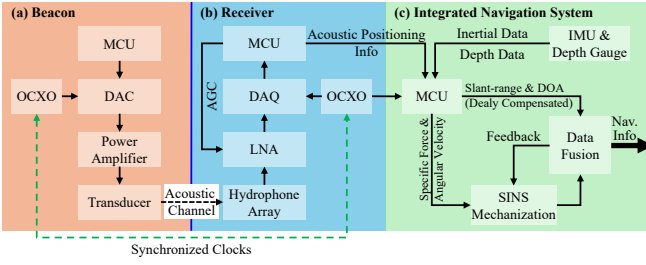


Fig. 2. The diagram of the SINS/piUSBL/depth gauge tightly coupled navigation system with time synchronization.

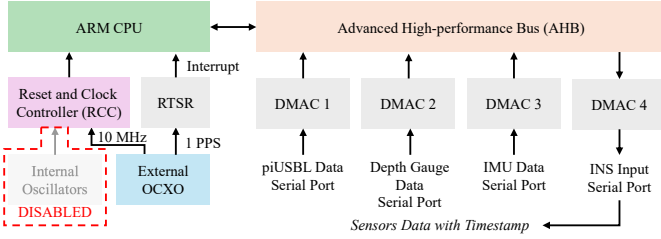


Fig. 3. The architecture of the microcontroller unit (MCU) with the OCXO for time synchronization.

on a static platform, such as a surface vessel, while the receiver is installed on a submersible that is integrated with a SINS unit. Both the beacon and the receiver are equipped with synchronized clocks, such as the oven-controlled crystal oscillator (OCXO) used in this study, which cost approximately 100 USD. Prior to mission execution, the clocks on both sides are disciplined using a high-precision GNSS time source to ensure precise time alignment and synchronization.

The OCXO generates a one pulse-per-second (1 PPS) signal, which is used to trigger the beacon to transmit an acoustic signal at the beginning of each second and the receiver synchronizes its sampling process with this signal. A matched filter is then applied by the onboard processor to detect the signal's time of flight (TOF), followed by conventional beamforming to estimate the azimuth of the beacon. After signal processing, the slant range and azimuth are transmitted to the SINS system for measurement updates. In time t_0 , the OCXO triggers the beacon to transmit an acoustic signal and simultaneously initiates the receiver's sampling process, respectively. Time t_1 marks the moment when the receiver detects the beginning of the incoming signal, while time t_2 indicates the end of the designed signal length. The sampling continues until time t_3 , which marks the end of the sampling window. Finally, the processed results are delivered to the SINS system at time t_4 . In the time t_1 , the paper defines that the TOF and direction of arrival (DOA) can be determined, even if the emission signal is not be fully record. Thus, the delay measured can be defined as the period between t_1 to t_4 .

The architecture of the piUSBL acoustic positioning system with OCXO, detailed in [30], [31], along with its integration with the SINS, is illustrated in Fig. 2. In the integrated navigation system, an STM32 microcontroller unit (MCU) is responsible for managing timestamps across multiple sensors, including a fiber-optic gyroscope (FOG)-based IMU, a depth

gauge, and the piUSBL acoustic positioning system.

The OCXO from the piUSBL system provides a highly stable clock reference for the integrated navigation system, particularly serving as the primary timing source for the MCU, as illustrated in Fig. 3. For the MCU, its internal oscillator is replaced by the external 10 MHz square-wave signal generated by the OCXO, which functions as the high-speed external oscillator (HSE) for system clock generation. Furthermore, the OCXO outputs a 1 PPS signal that triggers both the piUSBL system's transmission and sampling processes, and the MCU's rising-edge trigger selection register (RTSR) to generate an external interrupt. What's more, the OCXO also provides a 1 PPS signal output, which is used to trigger the piUSBL system transmitting and sampling, and the MCU's rise trigger select register (RTSR) to trigger an external interrupt on the rising edge of the 1 PPS signal. Upon receiving the 1 PPS signal, the central processing unit (CPU) records the corresponding timestamp, which corresponds to the time of sampling start within the piUSBL system. Meanwhile, the advanced high-performance bus (AHB) receives sensor data via the direct memory access controller (DMAC), including measurements from the piUSBL, depth gauge, and IMU, and transfers them to the MCU for timestamp alignment and subsequent output. Through clock synchronization between the piUSBL system and the SINS, the timestamps of the acoustic measurements can be precisely aligned with external sensor data, thereby enabling accurate time-delay measurement and compensation.

III. METHODOLOGY

The integration of synchronized clocks enables the system to record accurate timing information across various components. This section describes how these timestamps are used to calculate and handle the acoustic delay, and how the piUSBL observations are incorporated into the SINS for measurement updates.

A. Precise Time Delay Measurements

In practice, a significant time delay exists between the reception of the acoustic signal and the availability of the computed position from the piUSBL system.

As mentioned in Fig. 1, the interval $t_2 - t_1$ corresponds to the designed signal length, typically 20 ms in this study. Sampling continues until time t_3 , marking the end of the sampling window. The duration of this window ($t_3 - t_0$) is determined by the maximum expected range of the piUSBL system, which is typically set to 2 seconds during sea trials. The onboard processor applies matched filtering and beamforming to the sampled data to estimate the slant range and azimuth to the beacon. The processed results are then delivered to the SINS system at time t_4 .

As shown in Fig. 4, at time t_1 , the AUV is located at position p_1 , which corresponds to the ideal position associated with the piUSBL measurement z_0 . However, the slant range and azimuth are not available until time t_4 , when the processed measurement z_1 corresponds to the AUV's position p_4 . In this paper, the delay of the piUSBL system is defined as the time difference between the actual measurement time and the time

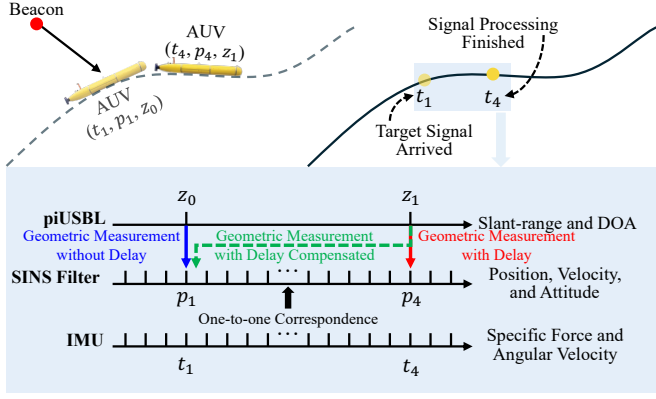


Fig. 4. The delay illustration of the SINS/piUSBL tightly coupled navigation system.

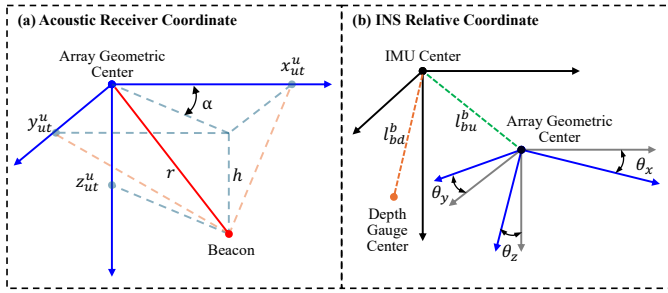


Fig. 5. The Coordinate System of the tightly coupled navigation system.

when the measurement becomes available, which is expressed as:

$$\Delta t = t_4 - t_1 \quad (1)$$

In practical applications, due to time synchronization, the true timestamp of the piUSBL measurement used in the SINS filter can be computed as:

$$t_1 = t_0 + t_{\text{tof}} \quad (2)$$

Here, t_0 is the time when the PPS signal is received and recorded by the MCU, and t_{tof} is the time of flight (TOF) of the acoustic signal, which can be obtained from the matched filtering process.

Once the true timestamp t_1 is accurately determined, the filtering reconstruction method is employed to address the delay issue within the navigation filter.

B. SINS/piUSBL Tightly Coupled Navigation

The involved reference frames in the following sections are the inertial frame (denoted as i -frame), the earth-centered-earth-fixed (ECEF) frame (denoted as e -frame), the navigation frame (denoted as n -frame), the body frame (denoted as b -frame), the depth gauge frame (denoted as d -frame), and the piUSBL frame (denoted as u -frame). These frames follow the community convention where it can be found in [32].

Fig. 5 illustrates the observation model of the piUSBL system and the relative positions of the IMU, piUSBL, and depth gauge. In Fig. 5 (a), the piUSBL provides two types of

observations in the u -frame: the slant range r and the azimuth α of the beacon. It is worth noting that, compared with the conventional USBL system described in [33], which provides two angular measurements and one slant range, the piUSBL system employed in this study lacks one angular measurement due to its planar circular array configuration. However, a single azimuth combined with the slant range is insufficient to fully determine the 3-dimensional position of the beacon in the u -frame. To address this limitation, a depth gauge is integrated into the tightly coupled navigation system to provide depth information for the submersible. As a compact and portable acoustic positioning solution, piUSBL has a limited effective range. Therefore, it is reasonable to assume that the horizontal plane remains approximately flat within the working area. Under the assumption that the beacon's position is known, and by combining the u -frame attitude, the vertical distance h in the u -frame can be readily calculated. The coordinates, $\mathbf{P}_{ut}^u = [x_{ut}^u, y_{ut}^u, z_{ut}^u]^\top$, represent the projected 3-dimensional position of the beacon in the u -frame and are computed as follows:

$$\begin{cases} x_{ut}^u = \sqrt{r^2 - h^2} \cos \alpha \\ y_{ut}^u = \sqrt{r^2 - h^2} \sin \alpha \\ z_{ut}^u = h \end{cases} \quad (3)$$

where h can be calculated as follows:

$$h = \mathbf{C}_b^u \mathbf{C}_n^b \mathbf{C}_e^n (h_t^e - h_e^e) \quad (4)$$

where the \mathbf{C}_b^u , \mathbf{C}_n^b , and \mathbf{C}_e^n are the direction cosine matrices (DCMs) representing the transformation from the b -frame to the u -frame, from the n -frame to the b -frame, and from the e -frame to the n -frame, respectively. The parameters h_t^e and h_e^e refer to the altitudes of the beacon and the hydrophone phase center of the piUSBL system in the e -frame, respectively.

As shown in Fig. 5(b), l_{bu}^b and l_{bd}^b represent the lever arms from the IMU to the piUSBL and the depth gauge, respectively, and both are expressed in the body frame. The piUSBL installation misalignment is modeled by the error vector $\delta\theta = [\theta_x, \theta_y, \theta_z]^\top$. The lever arms and installation misalignment are determined through precise calibration before deployment [34], [35].

Considering the aforementioned sources of error and the typical 21-dimensional error state equation of the INS [36], the error state of the tightly coupled navigation system can be expanded as follows:

$$\mathbf{X} = [\delta\mathbf{p}^n, \delta\mathbf{v}^n, \phi, \mathbf{g}_b, \mathbf{a}_b, \mathbf{g}_s, \mathbf{a}_s, \delta\theta, \delta k, \delta h^n]^\top \quad (5)$$

where $\delta\mathbf{p}^n$, $\delta\mathbf{v}^n$, and ϕ denote the position, velocity, and attitude errors in the navigation frame (n -frame), respectively. \mathbf{g}_b and \mathbf{a}_b represent the bias errors of the gyroscope and accelerometer, while \mathbf{g}_s and \mathbf{a}_s denote their corresponding scale factor errors. $\delta\theta$ denotes the installation misalignment error of the piUSBL system, δk is the scale factor error associated with the slant range measurement of the piUSBL, and δh^n represents the depth gauge measurement error in the n -frame.

The state transition matrix \mathbf{F} of the tightly coupled navigation system can be expressed as follows:

$$\mathbf{F} = \begin{bmatrix} \mathbf{F}_{\text{SINS}} & \mathbf{0}_{21 \times 4} & \mathbf{0}_{21 \times 1} \\ \mathbf{0}_{4 \times 21} & \mathbf{F}_{\text{piUSBL}} & \mathbf{0}_{4 \times 1} \\ \mathbf{0}_{1 \times 21} & \mathbf{0}_{1 \times 4} & \mathbf{F}_{\text{Depth}} \end{bmatrix} \quad (6)$$

where the SINS state transition matrix, \mathbf{F}_{SINS} , is described in [37]. The installation misalignment error $\delta\theta$, the slant range scale factor error δk , and the depth measurement error δh^n are assumed to be constant or slowly varying, with negligible dynamics. Therefore, their corresponding state transition matrices are modeled as zero: $\mathbf{F}_{\text{piUSBL}} = \mathbf{0}_{4 \times 4}$, $\mathbf{F}_{\text{Depth}} = \mathbf{0}$.

In the construction of measurement equations, the piUSBL system provides two types of measurements: the slant range r and the azimuth α , while the depth gauge provides the vertical distance h^n . The measurement equations can be expressed as follows:

$$\mathbf{Z} = \begin{bmatrix} \mathbf{Z}_{\text{piUSBL}} \\ \mathbf{Z}_{\text{Depth}} \end{bmatrix} = \begin{bmatrix} \hat{r}_{\text{SINS}} - \tilde{r}_{\text{piUSBL}} \\ \hat{\alpha}_{\text{SINS}} - \tilde{\alpha}_{\text{piUSBL}} \\ \hat{h}_{\text{SINS}}^n - \tilde{h}_{\text{Depth}}^n \end{bmatrix} = \mathbf{H}\mathbf{X} + \mathbf{V} \quad (7)$$

where \mathbf{Z} is the measurement vector, \hat{r}_{SINS} , $\hat{\alpha}_{\text{SINS}}$, and \hat{h}_{SINS}^n are the estimated slant range, azimuth, and depth, respectively. The tilde variables $\tilde{r}_{\text{piUSBL}}$, $\tilde{\alpha}_{\text{piUSBL}}$, and $\tilde{h}_{\text{Depth}}^n$ represent the actual measurements from the piUSBL system and the depth gauge, respectively. \mathbf{H} is the measurement matrix, and \mathbf{V} is the measurement noise vector.

Then, the measurement matrix \mathbf{H} in the tightly coupled navigation system is derived. Considering (3), the relationship between the coordinates of the beacon in the u -frame and the output of the piUSBL system is expressed as follows:

$$\begin{bmatrix} r \\ \alpha \end{bmatrix} = \begin{bmatrix} \sqrt{x_{ut}^u{}^2 + y_{ut}^u{}^2 + z_{ut}^u{}^2} \\ \arctan 2(y_{ut}^u, x_{ut}^u) \end{bmatrix} \quad (8)$$

Considering the lever arm from the IMU to the piUSBL, the coordinates of the beacon in the u -frame are expressed in terms of its coordinates in the b -frame as follows:

$$\mathbf{P}_{ut}^u = \mathbf{C}_b^u (\mathbf{P}_{bt}^b - \mathbf{l}_{bu}^b) \quad (9)$$

$$\begin{aligned} \hat{\mathbf{C}}_e^n &= \mathbf{C}_e^n + \delta\mathbf{C}_e^n \\ &= \begin{bmatrix} \sin(L + \delta L) \cos(\lambda + \delta\lambda) & -\sin(L + \delta L) \sin(\lambda + \delta\lambda) & \cos(L + \delta L) \\ -\sin(\lambda + \delta\lambda) & \cos(\lambda + \delta\lambda) & 0 \\ -\cos(L + \delta L) \cos(\lambda + \delta\lambda) & -\cos(L + \delta L) \sin(\lambda + \delta\lambda) & -\sin(L + \delta L) \end{bmatrix} \quad (16) \\ \delta\mathbf{C}_e^n &\approx \begin{bmatrix} -\delta L \cos L \cos \lambda + \delta\lambda \sin \lambda \sin L & -\delta\lambda \cos \lambda \sin L - \delta L \cos L \sin \lambda & -\delta L \sin L \\ -\delta\lambda \cos \lambda & -\delta\lambda \sin \lambda & 0 \\ \delta L \sin L \cos \lambda + \delta\lambda \sin \lambda \cos L & \delta L \sin L \sin \lambda - \delta\lambda \cos \lambda \cos L & -\delta L \cos L \end{bmatrix} \quad (17) \end{aligned}$$

Simplifying the second-order error term in (16), the error of the DCM from the e -frame to the n -frame can be expressed as (17), where δL and $\delta\lambda$ are the SINS latitude and longitude errors, respectively.

The Taylor expansion of (8) around the estimated position \mathbf{P}_{ut}^u is expressed as follows:

$$[\delta r \quad \delta\alpha]^\top = \mathbf{H}_a [\delta x_{ut}^u \quad \delta y_{ut}^u \quad \delta z_{ut}^u]^\top = \mathbf{H}_a \delta \mathbf{P}_{ut}^u \quad (10)$$

where \mathbf{H}_a is the Jacobian matrix, which can be expressed as follows:

$$\mathbf{H}_a = \begin{bmatrix} \frac{x_{ut}^u}{r} & \frac{y_{ut}^u}{r} & \frac{z_{ut}^u}{r} \\ -\frac{y_{ut}^u}{x_{ut}^u{}^2 + y_{ut}^u{}^2} & \frac{x_{ut}^u}{x_{ut}^u{}^2 + y_{ut}^u{}^2} & 0 \end{bmatrix} \quad (11)$$

According to (9), the partial derivative of \mathbf{P}_{ut}^u with respect to \mathbf{P}_{bt}^b can be given by:

$$\frac{\partial \mathbf{P}_{ut}^u}{\partial \mathbf{P}_{bt}^b} = \mathbf{C}_b^u \quad (12)$$

The error in \mathbf{P}_{ut}^u caused by the SINS error is analyzed. The coordinates of the beacon in the u -frame are expressed in the vector in the e -frame as follows:

$$\mathbf{P}_{ut}^u = \mathbf{C}_b^u \mathbf{C}_n^b \mathbf{C}_e^n \mathbf{P}_{ut}^e \quad (13)$$

where \mathbf{P}_{ut}^e represents the coordinates of the beacon in the e -frame, which are expressed as follows:

$$\begin{aligned} \mathbf{P}_{ut}^e &= \mathbf{r}_t^e - \mathbf{r}_b^e \\ &= \mathbf{r}_t^e - \mathbf{r}_b^e - \mathbf{C}_n^e \mathbf{C}_b^n \mathbf{l}_{bu}^b \\ &= \mathbf{P}_{bt}^e - \mathbf{C}_n^e \mathbf{C}_b^n \mathbf{l}_{bu}^b \end{aligned} \quad (14)$$

where \mathbf{P}_{bt}^e is the relative position from the body frame origin to the beacon in the e -frame, \mathbf{r}_t^e is the absolute position of the beacon in the e -frame, \mathbf{r}_b^e is the absolute position of the hydrophone phase center of the piUSBL system in the e -frame, and \mathbf{l}_{bu}^b is the lever arm from the IMU to the piUSBL in the b -frame.

By applying a perturbation to (13) and substituting (14) into it, the corresponding error expression is derived as:

$$\begin{aligned} \hat{\mathbf{P}}_{ut}^u &= \hat{\mathbf{C}}_b^u \hat{\mathbf{C}}_n^b \hat{\mathbf{C}}_e^n \hat{\mathbf{P}}_{ut}^e \\ &= \hat{\mathbf{C}}_b^u \hat{\mathbf{C}}_n^b \hat{\mathbf{C}}_e^n \hat{\mathbf{P}}_{bt}^e - \hat{\mathbf{C}}_b^u \mathbf{l}_{bu}^b \end{aligned} \quad (15)$$

We now proceed to expand each term individually.

Under the small-angle approximation, the perturbed DCM from the b -frame to the n -frame in the SINS is represented as:

$$\hat{\mathbf{C}}_n^b = \mathbf{C}_n^b (\mathbf{I} + \boldsymbol{\phi} \times) \quad (18)$$

where $\boldsymbol{\phi} \times$ is the skew-symmetric matrix of the attitude error vector $\boldsymbol{\phi}$.

Since the beacon's position \mathbf{r}_t^e and the lever arm \mathbf{l}_{bu}^b can be accurately measured, $\hat{\mathbf{P}}_{bt}^e$ can be expressed as:

$$\mathbf{r}_t^e = \begin{bmatrix} (R_N + h_t) \cos L_t \cos \lambda_t \\ (R_N + h_t) \cos L_t \sin \lambda_t \\ (R_M + h_t) \sin L_t \end{bmatrix} \quad (19)$$

$$\hat{\mathbf{r}}_b^e = \begin{bmatrix} (R_N + \hat{h}_b) \cos \hat{L}_b \cos \hat{\lambda}_b \\ (R_N + \hat{h}_b) \cos \hat{L}_b \sin \hat{\lambda}_b \\ (R_M + \hat{h}_b) \sin \hat{L}_b \end{bmatrix} \quad (20)$$

$$\hat{\mathbf{P}}_{bt}^e = \mathbf{r}_t^e - \hat{\mathbf{r}}_b^e \quad (21)$$

where R_N and R_M denote the radius of curvature of the earth in the prime vertical and meridian directions, respectively, h_t and h_b represent the altitudes of the beacon and the IMU in the n -frame, and the geographic latitude and longitude of the beacon are denoted as L_t and λ_t , while those of the IMU are denoted as \hat{L}_b and $\hat{\lambda}_b$, respectively.

The Taylor expansion of (20) around the SINS geographic position \mathbf{r}_b^n is expressed as follows:

$$\delta \mathbf{r}_b^e = \mathbf{H}_b [\delta L_b \quad \delta \lambda_b \quad \delta h_b]^\top = \mathbf{H}_b \delta \mathbf{r}_b^n \quad (22)$$

where $\delta \mathbf{r}_b^n = [\delta L_b, \delta \lambda_b, \delta h_b]^\top$ is the SINS geographic position error in the n -frame, and \mathbf{H}_b is the Jacobian matrix, which can be expressed as follows:

$$\mathbf{H}_b = \begin{bmatrix} \frac{\partial \mathbf{r}_b^e}{\partial L_b} & \frac{\partial \mathbf{r}_b^e}{\partial \lambda_b} & \frac{\partial \mathbf{r}_b^e}{\partial h_b} \end{bmatrix} \quad (23)$$

where the partial derivatives can be calculated as follows:

$$\frac{\partial \mathbf{r}_b^e}{\partial L_b} = \begin{bmatrix} -(R_N + h_b) \sin L_b \cos \lambda_b \\ -(R_N + h_b) \sin L_b \sin \lambda_b \\ (R_M + h_b) \cos L_b \end{bmatrix} \quad (24)$$

$$\frac{\partial \mathbf{r}_b^e}{\partial \lambda_b} = \begin{bmatrix} -(R_N + h_b) \cos L_b \sin \lambda_b \\ (R_N + h_b) \cos L_b \cos \lambda_b \\ 0 \end{bmatrix} \quad (25)$$

$$\frac{\partial \mathbf{r}_b^e}{\partial h_b} = \begin{bmatrix} \cos L_b \cos \lambda_b \\ \cos L_b \sin \lambda_b \\ \sin L_b \end{bmatrix} \quad (26)$$

$$\mathbf{H}_c = \begin{bmatrix} -\cos L_b \cos \lambda_b x_{bt}^e - \cos L_b \sin \lambda_b y_{bt}^e - \sin L_b z_{bt}^e & \sin \lambda_b \sin L_b x_{bt}^e - \cos \lambda_b \sin L_b y_{bt}^e & 0 \\ 0 & -\cos \lambda_b x_{bt}^e - \sin \lambda_b y_{bt}^e & 0 \\ -\sin L_b \cos \lambda_b x_{bt}^e + \sin L_b \sin \lambda_b y_{bt}^e - \cos L_b z_{bt}^e & \sin \lambda_b \cos L_b x_{bt}^e - \cos \lambda_b \cos L_b y_{bt}^e & 0 \end{bmatrix} \quad (35)$$

According to the above derivation, (32) is reexpressed as:

To ensure consistency with the system's error state definition, the geodetic position errors are transformed into the n -frame. (22) is expressed as follows:

$$\delta \mathbf{r}_b^e = \mathbf{H}_b \delta \mathbf{r}_b^n = \mathbf{H}_b \mathbf{D}_r^{-1} \delta \mathbf{p}_b^n \quad (27)$$

where the transformation matrix can be expressed as $\mathbf{D}_r^{-1} = \text{diag}(1/(R_M + h_b), 1/[(R_N + h_b) \cos L_b], -1)$.

Substituting (27) into (21) yields:

$$\hat{\mathbf{P}}_{bt}^e = \mathbf{P}_{bt}^e + \delta \mathbf{P}_{bt}^e = \mathbf{P}_{bt}^e - \mathbf{H}_b \mathbf{D}_r^{-1} \delta \mathbf{p}_b^n \quad (28)$$

Given that the piUSBL installation angles are sufficiently small, the DCM from the u -frame to the b -frame is linearized as:

$$\hat{\mathbf{C}}_b^u = (\mathbf{I} - \delta \boldsymbol{\theta} \times) \mathbf{C}_b^u \quad (29)$$

Substituting (16), (18), (28), and (29) into (15) yields:

$$\hat{\mathbf{P}}_{ut}^u = (\mathbf{I} - \delta \boldsymbol{\theta} \times) \mathbf{C}_b^u \mathbf{C}_n^b (\mathbf{I} + \boldsymbol{\phi} \times) (\mathbf{C}_e^n + \delta \mathbf{C}_e^n) (\mathbf{P}_{bt}^e + \delta \mathbf{P}_{bt}^e) - (\mathbf{I} - \delta \boldsymbol{\theta} \times) \mathbf{C}_b^u \mathbf{l}_{bu}^b \quad (30)$$

Ignoring the second-order error terms, the expression is simplified to:

$$\hat{\mathbf{P}}_{bt}^u \approx \mathbf{C}_b^u \mathbf{C}_n^b \mathbf{C}_e^n \mathbf{P}_{bt}^e - \mathbf{C}_b^u \mathbf{l}_{bu}^b + (\delta \boldsymbol{\theta} \times) \mathbf{C}_b^u \mathbf{l}_{bu}^b - (\delta \boldsymbol{\theta} \times) \mathbf{C}_b^u \mathbf{C}_n^b \mathbf{C}_e^n \mathbf{P}_{bt}^e + \mathbf{C}_b^u \mathbf{C}_n^b (\boldsymbol{\phi} \times) \mathbf{C}_e^n \mathbf{P}_{bt}^e + \mathbf{C}_b^u \mathbf{C}_n^b \delta \mathbf{C}_e^n \mathbf{P}_{bt}^e + \mathbf{C}_b^u \mathbf{C}_n^b \mathbf{C}_e^n \delta \mathbf{P}_{bt}^e \quad (31)$$

By combining the terms and rearranging, we derive:

$$\delta \mathbf{P}_{ut}^u \approx \left[(\mathbf{C}_b^u \mathbf{C}_n^b \mathbf{C}_e^n \mathbf{P}_{bt}^e) \times - (\mathbf{C}_b^u \mathbf{l}_{bu}^b) \times \right] \delta \boldsymbol{\theta} - \mathbf{C}_b^u \mathbf{C}_n^b [(\mathbf{C}_e^n \mathbf{P}_{bt}^e) \times] \boldsymbol{\phi} + \mathbf{C}_b^u \mathbf{C}_n^b (\delta \mathbf{C}_e^n \mathbf{P}_{bt}^e + \mathbf{C}_e^n \delta \mathbf{P}_{bt}^e) \quad (32)$$

Based on (17) and (28), the error term caused by position uncertainty is further decomposed as:

$$\mathbf{C}_e^n \delta \mathbf{P}_{bt}^e = \mathbf{C}_e^n (-\mathbf{H}_b \mathbf{D}_r^{-1} \delta \mathbf{p}_b^n) = -\mathbf{C}_e^n \mathbf{H}_b \mathbf{D}_r^{-1} \delta \mathbf{p}_b^n \quad (33)$$

$$\begin{aligned} \delta \mathbf{C}_e^n \mathbf{P}_{bt}^e &= \delta \mathbf{C}_e^n [x_{bt}^e \quad y_{bt}^e \quad z_{bt}^e]^\top \\ &= \mathbf{H}_c [\delta L_b \quad \delta \lambda_b \quad \delta h_b]^\top \\ &= \mathbf{H}_c \mathbf{D}_r^{-1} \delta \mathbf{p}_b^n \end{aligned} \quad (34)$$

where \mathbf{H}_c can be expressed as:

$$\begin{aligned} \delta \mathbf{P}_{ut}^u &\approx \mathbf{C}_b^u \mathbf{C}_n^b (\mathbf{H}_c - \mathbf{C}_e^n \mathbf{H}_b) \delta \mathbf{p}_b^n \\ &\quad - \mathbf{C}_b^u \mathbf{C}_n^b [(\mathbf{C}_e^n \mathbf{P}_{bt}^e) \times] \boldsymbol{\phi} \\ &\quad + \left[(\mathbf{C}_b^u \mathbf{C}_n^b \mathbf{C}_e^n \mathbf{P}_{bt}^e) \times - (\mathbf{C}_b^u \mathbf{l}_{bu}^b) \times \right] \delta \boldsymbol{\theta} \end{aligned} \quad (36)$$

Based on (7), the measurement innovation of the piUSBL system is further expressed as:

$$\mathbf{Z}_{\text{piUSBL}} = \begin{bmatrix} \hat{r}_{\text{SINS}} - \tilde{r}_{\text{piUSBL}} \\ \hat{\alpha}_{\text{SINS}} - \tilde{\alpha}_{\text{piUSBL}} \end{bmatrix} = \begin{bmatrix} \delta r_{\text{SINS}} - \delta r_{\text{piUSBL}} \\ \delta \alpha_{\text{SINS}} - \delta \alpha_{\text{piUSBL}} \end{bmatrix} \quad (37)$$

where δr and $\delta \alpha$ are the estimated or measured slant range and azimuth errors, respectively.

The piUSBL measurement error can be expressed as:

$$\begin{bmatrix} \delta r_{\text{piUSBL}} \\ \delta \alpha_{\text{piUSBL}} \end{bmatrix} = \begin{bmatrix} \delta k r + w_r \\ w_\alpha \end{bmatrix} \quad (38)$$

where δk is the slant range scale factor error, r is the slant range, and w_r and w_α are the measurement noises of the slant range and azimuth, respectively.

According to (10) and (36), the piUSBL measurement error obtained by the SINS is obtained as follows:

$$\begin{bmatrix} \delta r_{\text{SINS}} \\ \delta \alpha_{\text{SINS}} \end{bmatrix} = \begin{bmatrix} \mathbf{H}_p & \mathbf{H}_\phi & \mathbf{H}_\theta \end{bmatrix} \begin{bmatrix} \delta \mathbf{p}^n \\ \phi \\ \delta \theta \end{bmatrix} \quad (39)$$

where \mathbf{H}_p , \mathbf{H}_ϕ , and \mathbf{H}_θ can be expressed as follows:

$$\begin{cases} \mathbf{H}_p = \mathbf{C}_b^u \mathbf{C}_n^b (\mathbf{H}_c - \mathbf{C}_e^n \mathbf{H}_b) \\ \mathbf{H}_\phi = -\mathbf{C}_b^u \mathbf{C}_n^b [(\mathbf{C}_e^n \mathbf{P}_{bt}^e) \times] \\ \mathbf{H}_\theta = [(\mathbf{C}_b^u \mathbf{C}_n^b \mathbf{C}_e^n \mathbf{P}_{bt}^e) \times - (\mathbf{C}_b^u \mathbf{b}_{bu}^b) \times] \end{cases} \quad (40)$$

Substituting (38) and (39) into (37), we can obtain the piUSBL measurement innovation. Besides, the innovation of the depth gauge can be expressed as:

$$\begin{aligned} Z_{\text{Depth}} &= \hat{h}_{\text{SINS}}^n - \tilde{h}_{\text{Depth}}^n \\ &= h_{\text{SINS}}^n + \mathbf{e}_3 \left(\delta \mathbf{p}^n + [\mathbf{I} - (\phi \times)] \mathbf{C}_b^n \mathbf{l}_{bd}^b \right) \\ &\quad - (h_{\text{Depth}}^n + \delta h^n + w_h) \\ &= \mathbf{e}_3 \delta \mathbf{p}^n + \mathbf{e}_3 \left[(\mathbf{C}_b^n \mathbf{l}_{bd}^b) \times \right] \phi - \delta h^n - w_h \end{aligned} \quad (41)$$

where $\mathbf{e}_3 = [0, 0, 1]^\top$, \mathbf{H}_p , \mathbf{H}_ϕ , and \mathbf{H}_θ are expressed as follows:

$$\delta h_{\text{SINS}} = \begin{bmatrix} \mathbf{H}_h & \mathbf{H}_l \end{bmatrix} \begin{bmatrix} \delta \mathbf{p}^n \\ \phi \end{bmatrix} \quad (42)$$

where \mathbf{H}_h and \mathbf{H}_l can be expressed as:

$$\begin{cases} \mathbf{H}_h = \mathbf{e}_3 \\ \mathbf{H}_l = \mathbf{e}_3 \left[(\mathbf{C}_b^n \mathbf{l}_{bd}^b) \times \right] \end{cases} \quad (43)$$

In summary, the measurement transition matrix \mathbf{H} in the tightly coupled navigation system is expressed as:

$$\begin{aligned} \mathbf{H} &= \begin{bmatrix} \mathbf{H}_{\text{piUSBL}} \\ \mathbf{H}_{\text{Depth}} \end{bmatrix} \\ &= \begin{bmatrix} \mathbf{H}_p & \mathbf{0}_{2 \times 3} & \mathbf{H}_\phi & \mathbf{0}_{2 \times 12} & \mathbf{H}_\theta & -r & 0 \\ \mathbf{H}_h & \mathbf{0}_{1 \times 3} & \mathbf{H}_l & \mathbf{0}_{1 \times 12} & \mathbf{0}_{1 \times 3} & 0 & -1 \end{bmatrix} \end{aligned} \quad (44)$$

The above is the derivation process of the tightly coupled navigation system. Compared with the loosely coupled navigation system, the tightly coupled navigation system converts

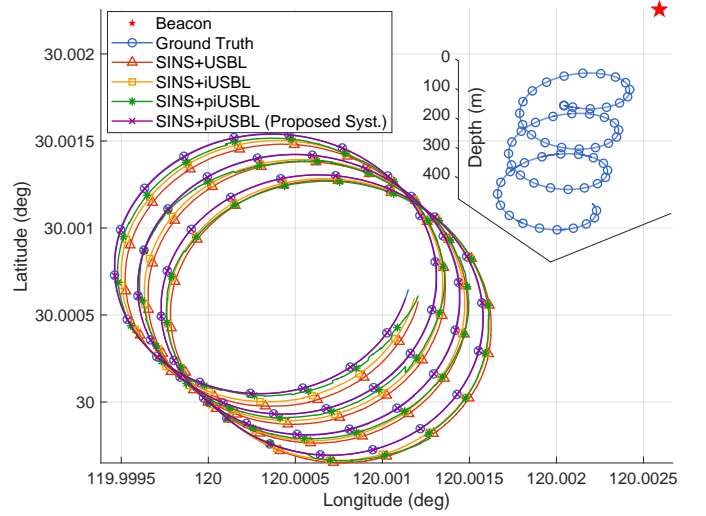


Fig. 6. Simulation trajectory curves.

the observation function from the position measurement to basic geometric measurements, like slant range and azimuth, which can avoid solution failure resulting from the loss or degradation of any individual measurement.

IV. SIMULATION AND FIELD EXPERIMENTS

To analyze the impact of time delay in underwater acoustic positioning sensors, and to validate both the proposed time-delay measurement method and the effectiveness of the proposed system, simulations and field experiments were conducted.

A. Simulation

To investigate the impact of time delay on performance in USBL, iUSBL, and piUSBL systems and the proposed tightly coupled navigation method, a series of simulation experiments were designed, as illustrated in Fig. 6.

The simulation trajectory follows a helical descent path, starting from the position (30°, 120°, 0 m). The AUV descends along a pitch angle of -15°, accelerating to 6 knots, and finally descending to a depth of 470 m. The beacon is positioned 250 m east and 250 m north of the origin. This simulation scenario effectively replicates a realistic underwater operation profile for an AUV during a mission involving continuous descent and motion. The sensor specifications used in the simulation are summarized in Table I.

It is worth noting that, in this simulation, we considered the acoustic communication delay, the positioning signal delay, and the processing delay of the USBL system, which corresponding to the t_1-t_4 in Fig. 1. Due to the inverted structure of the iUSBL and piUSBL systems, the acoustic communication delay is not considered in the iUSBL and piUSBL systems, as illustrated in Fig. 7. The USBL system exhibits a time delay that increases significantly with beacon distance, while the iUSBL system shows lower delays, though with a similarly increasing trend. In comparison, the piUSBL system has a similar delay magnitude to iUSBL, but due to the use of a

TABLE I
SIMULATION SPECIFICATIONS

Equipment	Specification	Accuracy
Gyroscope	Constant bias	0.01 deg/h
	Random walk	0.01 deg/ \sqrt{h}
	Scale factor error	50 ppm
Accelerometer	Constant bias	50 μg
	Random walk	0.01 m/s/ \sqrt{h}
	Scale factor error	100 ppm
USBL/iUSBL	Axis- x angle error	0.1 deg
	Axis- y angle error	0.1 deg
	Slant range (SR) error	0.1 % SR
	Measurement frequency	1 Hz
piUSBL	Azimuth error	0.1 deg
	Slant range (SR) error	0.1 % SR
	Measurement frequency	1 Hz

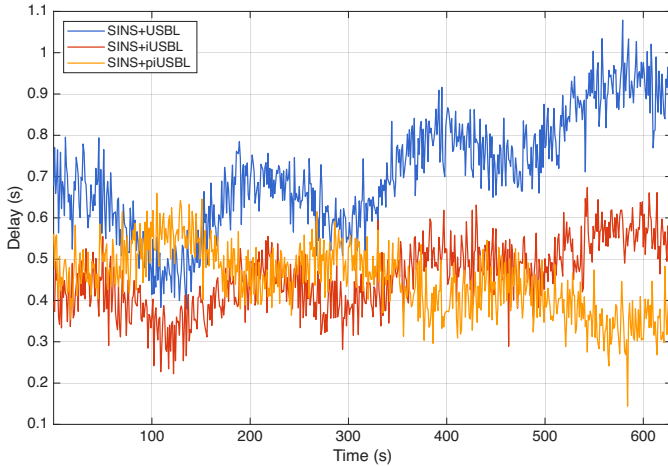


Fig. 7. Time delay error of the USBL, iUSBL, and piUSBL systems in simulation.

sampling window (see Eq. (1)), the closer the signal arrival is to the end of the window, the smaller the delay—leading to an inverse trend relative to the iUSBL system. The USBL and piUSBL systems are tightly coupled with the SINS. The structure of the system can be found in [38].

The simulation results, presented in Fig. 8 and Table II, show that the SINS/USBL system exhibits the largest position error, both in terms of root-mean-square error (RMSE) and maximum error (MAXERR), across the North, East, and Height/Down projections. This is primarily due to the significant time delay associated with the USBL system, compared to the iUSBL and piUSBL systems.

The SINS/iUSBL system demonstrates a smaller position error by eliminating the need for acoustic communication

TABLE II
POSITION ERROR OF THE FOUR SYSTEMS IN SIMULATION.

Sub Syst.	RMSE(m)			MAXERR(m)		
	e_N	e_E	e_D	e_N	e_E	e_D
USBL	5.65	5.06	0.55	8.41	6.59	0.76
iUSBL	3.78	3.42	0.35	5.55	4.41	0.47
piUSBL	3.12	3.14	0.42	6.37	6.65	3.23
Prop. Syst.	0.17	0.28	0.02	0.42	0.48	0.16

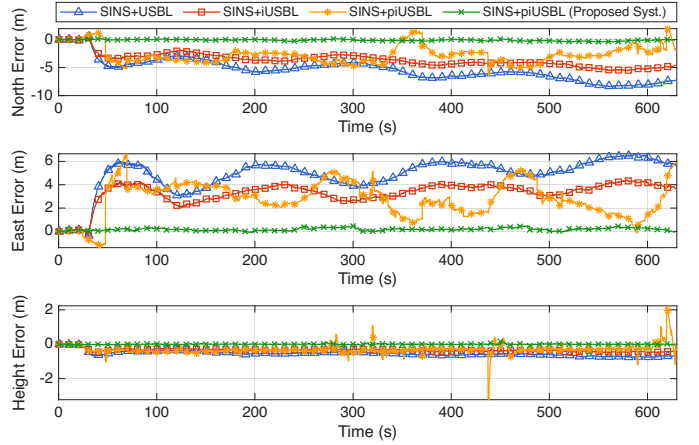


Fig. 8. Position error of the SINS/USBL, SINS/iUSBL, SINS/piUSBL, and proposed SINS/piUSBL with time delay accurate measurement aided integrated navigation system in simulation.

delay. Compared to the SINS/USBL system, the RMSE of the SINS/iUSBL system is reduced by 32.89%, from 7.61 m to 5.11 m, and the MAXERR is reduced by 33.65%, from 10.91 m to 7.11 m. It is important to note that, unless otherwise specified, both the RMSE and MAXERR are computed using the Euclidean norm.

The SINS/piUSBL system shows a slight reduction in position error in terms of RMSE, with a 41.52% reduction from 7.61 m to 4.45 m compared with SINS/USBL system. However, it is important to note that the SINS/piUSBL system has a larger MAXERR than the SINS/iUSBL system. This is because the piUSBL system lacks an angular measurement, which reduces its robustness to external disturbances and reveals a higher susceptible to time delay. As a result, when errors occur in the observations, the system's filter is destabilized, leading to fluctuations in the estimated position.

The proposed SINS/piUSBL system with accurate time delay measurement, referred to as the Prop. Syst. in Table II, demonstrates the smallest position error. The RMSE is reduced by 96.45%, from 7.61 m to 0.27 m, and the MAXERR is reduced by 93.95%, from 10.91 m to 0.66 m, compared with the SINS/USBL system.

In summary, the piUSBL-based integrated navigation system outperforms both the USBL and iUSBL systems in terms of average error, despite exhibiting significant oscillations when handling outliers caused by time delay. By introducing the proposed time delay error estimation method, this issue is effectively addressed, resulting in a significant improvement in the accuracy of the compensated piUSBL system.

B. Field Experiments

To further validate the performance of the proposed system and assess the effectiveness of accurate time delay measurement, field experiments were conducted.

The field experiment was conducted at the Tannong Reservoir, and its system structure is shown in Fig. 9. In the experimental setup, the acoustic beacon was fixed on the shore at a depth of 0.83 m underwater. The experimental platform was

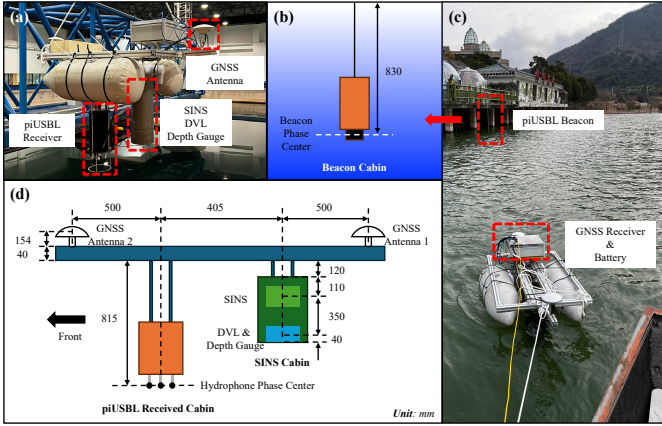


Fig. 9. Setup of the SINS/piUSBL system during field experiments.

TABLE III
FIELD EXPERIMENT SPECIFICATIONS

Equipment	Specification	Accuracy
Gyroscope	Constant bias	0.03 deg/h
	Random walk	$0.005 \text{ deg}/\sqrt{\text{h}}$
	Scale factor error	100 ppm
Accelerometer	Constant bias	$300 \mu\text{g}$
	Random walk	$0.05 \text{ m/s}/\sqrt{\text{h}}$
	Scale factor error	200 ppm
piUSBL	Depth error	0.1 deg
	Slant range (SR) error	0.1% SR
	Measurement frequency	1 Hz
OCXO	Clock drift ($\leq 2 \text{ hr}$)	$3 \mu\text{s/hr}$
	Clock drift ($> 2 \text{ hr}$)	$18 \mu\text{s/hr}$
Depth gauge	Depth error	0.1 m
DGNSS	Position error (CORS)	0.02 m

equipped with the piUSBL receiver system, SINS, DVL, depth gauge, and Differential Global Navigation Satellite System (DGNSS). The sensor performance parameters are provided in Table III.

The relative positions of the systems, as shown in Fig. 9(d), were accurately measured, with the values expressed in millimeters. The experiment was conducted by towing the platform with a small boat, as illustrated in Fig. 9(c).

Before the experiment, the OCXOs onboard the piUSBL system's transmitter and receiver were disciplined using a high-precision GNSS clock for 30 minutes. Based on the clock performance we employed, the time offset between the two clocks remained below $6 \mu\text{s}$ throughout the experiment. When the typical sound speed in freshwater is around 1500 m/s, the slant range error caused by the clock offset is less than 0.009 m, which is negligible compared to the piUSBL system's inherent measurement error.

The trajectory of the experiment is shown in Fig. 10. To verify the system's performance, we conducted experiments on the conventional SINS/piUSBL tightly coupled method as well as the proposed tightly coupled system based on precise time delay measurement. It is noteworthy that, based on our understanding of the experimental site, the northeast and south sides of the reservoir have shallower depths and more complex acoustic environments, which may lead to increased errors in

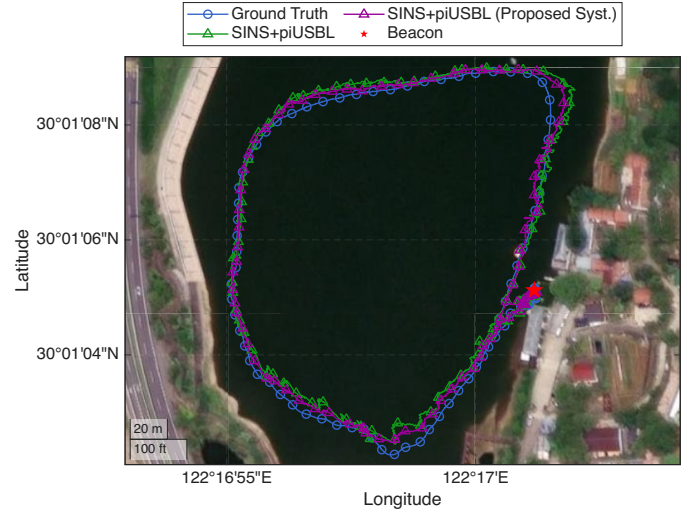


Fig. 10. Trajectory of the ground truth, SINS/piUSBL, and SINS/piUSBL with time delay accurate measurement aided integrated navigation system in field experiment.

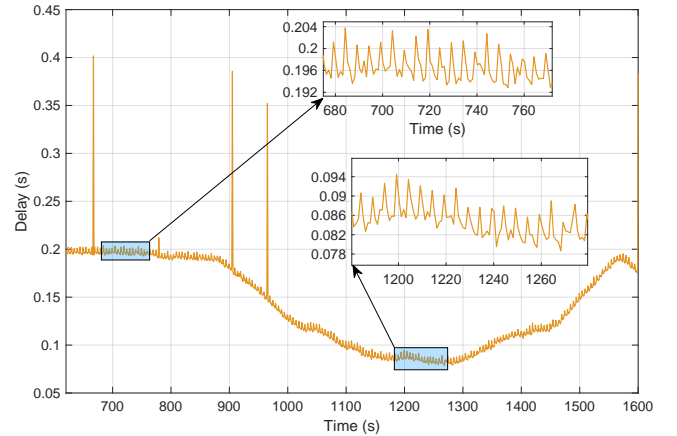


Fig. 11. Time delay error of the piUSBL systems in field experiments.

the acoustic system.

Fig. 11 shows the time delay measured using the synchronized clocks. The results clearly indicate that the delay is influenced by system processing delays and other factors, maintaining an amplitude of approximately 8 ms across different parts of the system. Additionally, the delay is observed to vary with the distance from the acoustic source. Furthermore, due to issues such as instability in serial communication, noticeable jumps in the delay are also evident. Based on these delay measurements, it is apparent that when a commonly used 200 Hz IMU is employed as the sensor in the INS, the presence of the delay results in piUSBL observations being delayed by tens of inertial measurement updates, which significantly impacts the accuracy of the system.

Fig. 12 shows the trajectory of the SINS/piUSBL tightly coupled method and the proposed tightly coupled navigation method based on precise time delay measurement and compensation projected onto the navigation frame. The ground truth is obtained using the DGNSS system, which provides high-precision position information. Fig. 13 illustrates the error

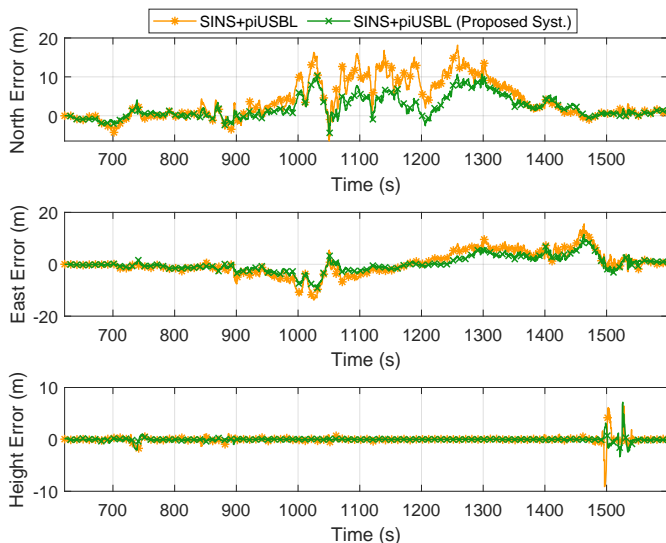


Fig. 12. Position error of the SINS/piUSBL and SINS/piUSBL with time delay accurate measurement aided integrated navigation system in field experiment.

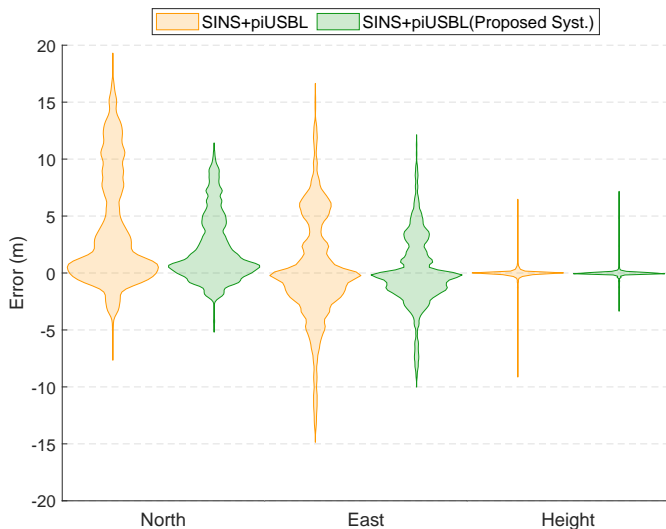


Fig. 13. Violin plot of field experiment's position error between the SINS/piUSBL and the SINS/piUSBL with time delay accurate measurement aided integrated navigation system in the north, east and height directions.

distribution with violin plots. The position errors in the north and east directions clearly shift towards a mean of zero after time delay compensation. The height error, which is constrained by the depth gauge, shows minimal variation overall. Compared in the maximum error, the proposed system shows a significant reduction in maximum error in all three directions. Regarding the RMSE of position errors, which is given in Table IV, the proposed tightly coupled navigation system, with accurate time delay measurement and compensation, improves the position errors in the north, east, and vertical directions by 44.02%, 34.23%, and 33.82%, respectively, compared to the system with time delays. The overall precision is improved by 40.45%, reducing from 7.72 m to 4.59 m. Furthermore, the accurate experimental measurements and compensation significantly reduce the maximum errors in all three directions,

TABLE IV
POSITION ERROR FOR SINS/piUSBL SYSTEM WITH AND WITHOUT DELAY COMPENSATION.

INS Syst.	RMSE (m)			MAXERR (m)		
	e_N	e_E	e_D	e_N	e_E	e_D
Without Comp.	6.27	4.44	0.68	18.14	15.57	9.11
With Comp.	3.51	2.92	0.45	10.74	11.47	7.15
Improvement(%)	44.02	34.23	33.82	40.79	26.33	21.51

with maximum errors decreasing by 40.79%, 26.33%, and 21.51%, respectively. The overall maximum error is reduced by 32.55%, from 25.59 m to 17.26 m.

The results of the field experiment demonstrate that the proposed SINS/piUSBL tightly coupled navigation system is capable of performing integrated navigation under minimal constraints, even in the absence of one angular observation. Furthermore, the proposed OCXO-based time delay measurement method effectively measures the system's time delay and has been validated in the integrated navigation system. Compared to the system without time delay compensation, the navigation accuracy showed significant improvements in both RMSE and MAXERR metrics, which also align with the results obtained from the simulation.

V. CONCLUSIONS

The time delay in the sensor fusion process of navigation systems has a significant impact on system accuracy. To address this issue, this paper proposes a SINS/piUSBL/depth gauge underwater integrated navigation system based on precise time delay measurement. The system incorporates the synchronized clock of the piUSBL into the fusion architecture, thereby aligning acoustic signal reception, processing, and computation with the SINS time base, and achieving an effectively "delay-aware" integrated navigation scheme. The proposed framework has been validated through both simulations and field experiments. The following conclusions are drawn:

- 1. Characterization of delay effects:** This study provides a systematic analysis of the impact of time delay in acoustic-aided navigation systems. It reveals that delay-induced errors arise primarily from the mismatch between the actual measurement epoch and the fusion epoch. Comparative simulations of USBL, iUSBL, and piUSBL show that, due to inherent operational mechanisms, the delays in iUSBL and piUSBL are substantially smaller than those of USBL, with piUSBL exhibiting the lowest intrinsic delay. The results also indicate that while piUSBL slightly outperforms iUSBL in terms of average position error, its maximum error can be more pronounced due to the lack of vertical-angle observability.
- 2. Minimal observation integration:** Based on the self-designed piUSBL system, a tightly coupled underwater navigation method integrating SINS, piUSBL, and depth gauge with minimal observations is developed and theoretically derived. By eliminating one angular measurement compared with traditional acoustic schemes, the framework reduces system complexity while retaining

observability. This formulation provides a theoretical reference for extending simplified and low-cost acoustic devices into integrated navigation systems.

3. **Systematic delay modeling with OCXO:** Building on the previous two, we introduce the OCXO carried by the piUSBL system into the entire navigation system. By leveraging synchronized clocks, the proposed approach establishes a systematic framework for quantifying and compensating acoustic system delays throughout the entire operational process. This enables the time delay, traditionally difficult to observe and correct in underwater navigation, to be explicitly measured and effectively mitigated within the integrated system. Field experimental results show that after accurate time delay measurement and compensation, the RMSE of the navigation position improved by 40.45%, and the MAXERR decreased by 32.55%. These results are consistent with the trends observed in the simulation.

Due to the limitations of experimental equipment and conditions, further studies with more accurate and realistic experimental setups are necessary. Future research will focus on expanding the application of this method to a broader range of acoustic systems in integrated navigation. Additionally, it will explore the potential of this approach to improve the precision of underwater integrated navigation systems based on acoustic technologies. Specifically, this work paves the way for deeper coupling of the raw data from the acoustic system and the inertial navigation system, facilitating tighter integration of both systems. This advancement will significantly enhance the system's robustness and accuracy, offering a promising solution for high-precision underwater navigation across various applications.

REFERENCES

- [1] D. Ma, Y. Li, T. Ma, and A. M. Pascoal, "The state of the art in key technologies for autonomous underwater vehicles: A review," *Engineering*, 2025.
- [2] H. Li, Z. Liu, J. Huang, X. An, and Y. Chen, "An improved es-based line-of-sight guidance law for path following of underactuated autonomous underwater helicopter with nonlinear tracking differentiator and anti-saturation controller," *Ocean Engineering*, vol. 322, p. 120456, 2025.
- [3] L. Paull, S. Saeedi, M. Seto, and H. Li, "Auv navigation and localization: A review," *IEEE Journal of Oceanic Engineering*, vol. 39, no. 1, pp. 131–149, 2014.
- [4] B. Zhang, D. Ji, S. Liu, X. Zhu, and W. Xu, "Autonomous underwater vehicle navigation: A review," *Ocean Engineering*, vol. 273, p. 113861, 2023.
- [5] P. Chen, Y. Li, Y. Su, X. Chen, and Y. Jiang, "Review of auv underwater terrain matching navigation," *Journal of Navigation*, vol. 68, no. 6, pp. 1155–1172, 2015.
- [6] P. A. Miller, J. A. Farrell, Y. Zhao, and V. Djapic, "Autonomous underwater vehicle navigation," *IEEE Journal of Oceanic Engineering*, vol. 35, no. 3, pp. 663–678, 2010.
- [7] Y. Yao, X. Xu, X. Xu, and I. Klein, "Virtual beam aided sins/dvl tightly coupled integration method with partial dvl measurements," *IEEE Transactions on Vehicular Technology*, vol. 72, no. 1, pp. 418–427, 2023.
- [8] F. Maurelli, S. Krupiński, X. Xiang, and Y. Petillot, "Auv localisation: A review of passive and active techniques," *International Journal of Intelligent Robotics and Applications*, vol. 6, no. 2, pp. 246–269, 2022.
- [9] L. Zhang, L.-T. Hsu, and T. Zhang, "A novel ins/usbl integrated navigation scheme via factor graph optimization," *IEEE Transactions on Vehicular Technology*, vol. 71, no. 9, pp. 9239–9249, 2022.
- [10] W. Zhao, S. Qi, R. Liu, G. Zhang, and G. Liu, "A review of underwater multi-source positioning and navigation technology," in *Lecture Notes in Electrical Engineering*, ser. Lecture Notes in Electrical Engineering, L. Yan, H. Duan, and Y. Deng, Eds. Singapore: Springer Nature, 2023, pp. 5466–5479.
- [11] K. Vickery, "Acoustic positioning systems. new concepts-the future," in *Proceedings of the 1998 Workshop on Autonomous Underwater Vehicles (Cat. No.98CH36290)*, 1998, pp. 103–110.
- [12] N. R. Rypkema, E. M. Fischell, and H. Schmidt, "One-way travel-time inverted ultra-short baseline localization for low-cost autonomous underwater vehicles," in *2017 IEEE International Conference on Robotics and Automation (ICRA)*. IEEE, 2017, pp. 4920–4926.
- [13] H. Guo, Z. Qian, X. Wang, W. Sun, L. Jie, and J. Zhai, "A robust attitude estimation algorithm for seabed inverted ultra-short baseline," *Ocean Engineering*, vol. 280, p. 114534, 2023.
- [14] X. Yu, H.-D. Qin, and Z.-B. Zhu, "Underwater localization of auvs in motion using two-way travel time measurements with unknown sound velocity," *IEEE Transactions on Vehicular Technology*, vol. 72, no. 9, pp. 11358–11373, 2023.
- [15] N. R. Rypkema and H. Schmidt, "Passive inverted ultra-short baseline (piusbl) localization: An experimental evaluation of accuracy," in *2019 IEEE/RSJ International Conference on Intelligent Robots and Systems (IROS)*. IEEE, 2019, pp. 7197–7204.
- [16] H. Zhao, Z. Gong, J. Yan, C. Li, and X. Guan, "Unsynchronized underwater localization with isogradient sound speed profile and anchor location uncertainties," *IEEE Transactions on Vehicular Technology*, vol. 73, no. 6, pp. 8864–8877, 2024.
- [17] P. Ridao, D. Ribas, E. Hernandez, and A. Rusu, "Usbl/dvl navigation through delayed position fixes," in *2011 IEEE International Conference on Robotics and Automation*, 2011, pp. 2344–2349.
- [18] T. I. Fossen, "Feedback error-state kalman filter with time-delay compensation for hydroacoustic-aided inertial navigation of underwater vehicles," *Control Engineering Practice*, vol. 138, p. 105603, 2023.
- [19] M. Xia, T. Zhang, L. Zhang, B. Yang, and Y. Shi, "A mixture distribution-based robust sins/usbl integration navigation with time-varying delays," *Measurement Science and Technology*, vol. 32, no. 1, p. 015903, 2021.
- [20] G. Wang, S. Hu, M. Liu, J. Cui, Z. Peng, and J.-H. Cui, "Adaptive unscented kalman filtering and signal-sending time estimation for calibration of sins/usbl navigation system," *IEEE Transactions on Instrumentation and Measurement*, vol. 74, pp. 1–12, 2025.
- [21] S. Liu, T. Zhang, J. Zhang, and M. Xia, "A robust tightly sins/usbl based auv localization method aided by dual transponder," *Measurement*, vol. 223, p. 113725, 2023.
- [22] B. Xu, H. Zhu, and Y. Guo, "A robust iterative algorithm for sins/usbl integrated navigation based on dual hydrophone differential model," *Measurement*, vol. 242, p. 115854, 2025.
- [23] A. Comellini, D. Casu, E. Zenou, V. Dubanchet, and C. Espinosa, "Incorporating delayed and multirate measurements in navigation filter for autonomous space rendezvous," *Journal of Guidance, Control, and Dynamics*, vol. 43, no. 6, pp. 1164–1172, 2020.
- [24] B. Xu, X. Wang, J. Zhang, A. A. Razzaqi, B. Xu, X. Wang, J. Zhang, A. A. Razzaqi, B. Xu, X. Wang, J. Zhang, A. A. Razzaqi, B. Xu, X. Wang, J. Zhang, and A. A. Razzaqi, "Maximum correntropy delay kalman filter for sins/usbl integrated navigation," *ISA Transactions*, vol. 117, pp. 274–287, 2021.
- [25] D. Ribas, P. Ridao, A. Mallios, and N. Palomeras, "Delayed state information filter for usbl-aided auv navigation," in *2012 IEEE International Conference on Robotics and Automation*, 2012, pp. 4898–4903.
- [26] G. Xiao, B. Wang, Z. Deng, M. Fu, and Y. Ling, "An acoustic communication time delays compensation approach for master-slave auv cooperative navigation," *IEEE Sensors Journal*, vol. 17, no. 2, pp. 504–513, 2017.
- [27] B. Xu, J. Zhang, and A. A. Razzaqi, "A novel robust filter for outliers and time-varying delay on an sins/usbl integrated navigation model," *Measurement Science and Technology*, vol. 32, no. 1, p. 015903, 2021.
- [28] X. Wang, Y. Wei, and H. Shao, "An information fusion algorithm for ins/dvl/usbl integrated navigation system based on delay state unscented kalman filter," in *2023 IEEE International Conference on Mechatronics and Automation (ICMA)*, vol. 32, 2023, pp. 1161–1166.
- [29] N. R. Rypkema, "Underwater & out of sight : Towards ubiquity in underwater robotics," Thesis, Massachusetts Institute of Technology, 2019.
- [30] Y. Wang, S. H. Huang, Z. Wang, R. Hu, M. Feng, P. Du, W. Yang, and Y. Chen, "Design and experimental results of passive iusbl for small auv navigation," *Ocean Engineering*, vol. 248, p. 110812, 2022.

- [31] Y. Wang, R. Hu, S. H. Huang, Z. Wang, P. Du, W. Yang, and Y. Chen, "Passive inverted ultra-short baseline positioning for a disc-shaped autonomous underwater vehicle: Design and field experiments," *IEEE Robotics and Automation Letters*, vol. 7, no. 3, pp. 6942–6949, 2022.
- [32] P. D. Groves, *Principles of GNSS, Inertial, and Multisensor Integrated Navigation Systems, Second Edition*. Artech House, 2013.
- [33] G. Wang, S. Hu, M. Liu, J. Cui, Z. Peng, and J.-H. Cui, "Adaptive unscented kalman filtering and signal-sending time estimation for calibration of sins/usbl navigation system," *IEEE Transactions on Instrumentation and Measurement*, vol. 74, pp. 1–12, 2025.
- [34] Y. Yao, X. Xu, D. Yang, and X. Xu, "An imm-ukf aided sins/usbl calibration solution for underwater vehicles," *IEEE Transactions on Vehicular Technology*, vol. 69, no. 4, pp. 3740–3747, 2020.
- [35] J. Huang, H. Li, Z. Liu, Z. Wang, Y. Wang, and Y. Chen, "Gnss-aided installation error compensation for dvl/ins integrated navigation system using error-state kalman filter," *Measurement*, vol. 242, p. 116224, 2025.
- [36] X. Niu, Q. Zhang, L. Gong, C. Liu, H. Zhang, C. Shi, J. Wang, and M. Coleman, "Development and evaluation of gnss/ins data processing software for position and orientation systems," *Survey Review*, vol. 47, no. 341, pp. 87–98, 2015.
- [37] D. Titterton and J. Weston, *Strapdown Inertial Navigation Technology*. IET Digital Library, 2004.
- [38] D. Wang, B. Wang, H. Huang, Y. Yao, and X. Xu, "Robust filter method for sins/dvl/usbl tight integrated navigation system," *IEEE Sensors Journal*, vol. 23, 2023.